DOI: 10.1002/ejic.200((will be filled in by the editorial staff))

Crystal phase and morphology controlled synthesis of Fe_2O_3 nanomaterials

Xiaoling Mou,[a] Yong Li,[a] Bingsen Zhang,[b] Lide Yao,[c] Xuejiao Wei,[a] Dang Sheng Su* [b,c] and Wenjie Shen*[a]

Keywords: Crystal Phase / Morphology / Fe_2O_3 / Nanorods / NO+CO

Alpha- and gamma-Fe_2O_3 nanorods have been prepared from a β-FeOOH precursor that was obtained by aqueous-phase precipitation of ferric chloride. The oxyhydroxide precursor had a rod-like shape with the diameter of 30-40 nm and the length of 400-500 nm. Calcination at 500 °C of the rod-shaped oxyhydroxide in air yielded α-Fe_2O_3 nanorods whereas refluxing in PEG at 200 °C resulted in the formation of γ-Fe_2O_3 nanorods. Both oxides inherited the precursor's rod-like morphology but exposed different crystalline facets. When being used to catalyze NO reduction by CO, an environmentally important reaction in NO abatement, the γ-Fe_2O_3 nanorods were much more active than the α-Fe_2O_3 nanorods, showing an apparent crystal phase effect. This was because that the γ-Fe_2O_3 nanorods simultaneously exposed iron and oxygen ions on the surfaces that facilitated the adsorption and activation of NO and CO molecules.

[a] State Key Laboratory of Catalysis, Dalian Institute of Chemical Physics,Chinese Academy of Sciences, Dalian 116023, China.
Fax: +86-411-8469-4447
E-mail: shen98@dicp.ac.cn
[b] Shenyang National Laboratory for Materials Science, Institute of Metal Research, Chinese Academy of Sciences, Shenyang 110016, China.
[c] Department of Inorganic Chemistry, Fritz-Haber Institute of the Max Planck Society, D-14195 Berlin, Germany.
Fax: +49-30-8413-4401
E-mail: dangsheng@fhi-berlin.mpg.de

Introduction

In recent years, there is great interest in nanostructured Fe_2O_3 (also known as ferric oxide) materials for both fundamental and practical reasons. To date, four crystalline polymorphs of ferric oxides have been well described: α-, β-, γ- and ε-Fe_2O_3.[1] Based on their different crystalline structures, each of the Fe_2O_3 polymorphs has unique biochemical, magnetic, and catalytic properties, especially at the nanometer level.[1-2] Among them, the highly crystalline alpha- and gamma-Fe_2O_3 that occur in nature are the most interesting and potentially useful phases. In addition to the widespread use in magnetic recording industry,[3] α-Fe_2O_3 was also used as heterogeneous catalysts[4] and more recently has been applied to solar cells for the photocatalytic splitting of water,[5] while γ-Fe_2O_3 nanostructures have been extensively examined for medical applications.[6] In order to tune their crystal phase, size and morphology that may greatly alter their physicochemical properties, considerable efforts have been expended on fabricating Fe_2O_3 nanomaterials, mostly in the form of nanoparticles, nanorods, nanowires, and nanotubes.

Fabrication of small Fe_2O_3 nanoparticles with high surface to volume ratio was the focus in early studies. α-Fe_2O_3 particles with diameters as small as 4 nm[7] and nanocubes with an average length of 15 nm[8] have been successfully synthesized in liquid phase. Meanwhile, γ-Fe_2O_3 nanoparticles have also been prepared with the diameter of less than 5 nm.[9] Quite recently, crystal phase and shape control of Fe_2O_3 nanomaterials is of utmost importance in materials science. For α-Fe_2O_3, one-dimensional nanostructures, like nanorods,[10] nanochains,[11] nanotubes,[12] and nanowires,[13] were successfully synthesized using solution-based approaches. Short α-Fe_2O_3 nanorods with a mean diameter of 5.2 nm and an average length of 16.8 nm were prepared through a sol-gel method.[10a] Starting from a simple Fe-H_2O system, α-Fe_2O_3 nanorods with a length of a few micrometers and an average diameter of 20 (tip) to 100 nm (base) were fabricated as well.[14] Typically, most of the α-Fe_2O_3 nanorods were prepared from α- or β-FeOOH precursors that were usually synthesized by hydrolysis of ferric ions in liquid solution. For example, calcination of α- and β-FeOOH in air yielded α-Fe_2O_3 nanorods with the diameter of 20-300 nm and the length of 200-1000 nm.[15] Similarly, porous α-Fe_2O_3 nanorods with the diameter of 38 nm and the length of 480 nm were obtained by heating a rod-like β-FeOOH precursor that had been prepared by precipitation of $FeCl_3$ with urea in aqueous solution.[16] On the other hand, tailoring of γ-Fe_2O_3 nanostructures is still somewhat difficult because the most commonly used hard template approach often resulted in the formation of large sizes. For instance, γ-Fe_2O_3 nanowires (50~90 nm in width and 10~20 μm in length) was obtained by polymorphous transformation of α-Fe_2O_3 nanowires,[17] and γ-Fe_2O_3 nanotubes with a length of 30 μm and a wall thickness of 20 nm (outer diameter about 400 nm) have been fabricated using anodic aluminum oxide (AAO) as the hard template.[18] To minimize the dimension of these nanostructures, thermal decomposition of $Fe(CO)_5$ in liquid phase has been recently used to prepare γ-Fe_2O_3 diamonds, triangles and spheres with the sizes being smaller than 20 nm under the assistance of dodecylamine (DDA) as the capping agent.[19]

On the other hand, the high-temperature treatment involved in most synthetic strategies often triggers diverse polymorphous transitions that yield undesired mixtures of Fe_2O_3 polymorphs, instead of a single-crystalline phase. Since α-Fe_2O_3 is the final product of thermally induced transformations of Fe_2O_3 polymorphs, its size and shape control is relatively easier than that of γ-Fe_2O_3. In general, there still remains a challenge for precious tailoring the shape and the crystal phase of Fe_2O_3 nanomaterials simultaneously using facile and environment benign approaches. In this work, we have successfully fabricated α- and γ-Fe_2O_3 nanorods using a β-FeOOH precursor that was obtained by precipitation of ferric

chloride in aqueous solution. The rod-shaped Fe_2O_3 nanomaterials showed apparent crystal phase effect in catalytic reduction of NO by CO.

Results and Discussion

Figure 1a shows the XRD pattern of the β-FeOOH precursor, where the typical diffraction lines corresponded to well-crystallized β-FeOOH (ICSD 31136). In the FTIR spectrum (Figure 2a), the intense bands at 628 and 700 cm^{-1} represented the characteristic vibrations of Fe-O and the minor band at 419 cm^{-1} was assigned to the symmetric vibration of Fe-O-Fe.[20] The weak band at 814 cm^{-1} was attributed to OH-blending.[21] Figure 3 shows the SEM/TEM images of the as-prepared β-FeOOH. It is obvious that the β-FeOOH had a uniform rod-like morphology with smooth surface and rectangular tip. The diameter was 30-40 nm and the length ranged from 400 to 500 nm.

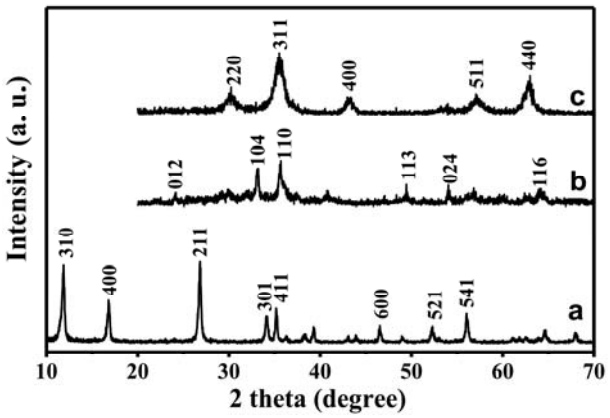

Figure 1. XRD patterns of (a) the β-FeOOH precursor, (b) the α-Fe_2O_3 nanorods, and (c) the γ-Fe_2O_3 nanorods.

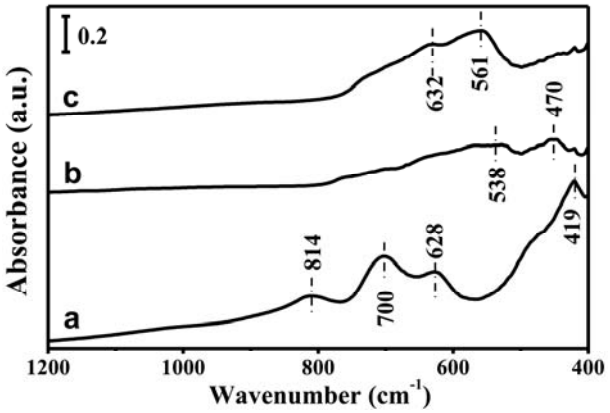

Figure 2 FTIR spectra of (a) the β-FeOOH precursor, (b) the α-Fe_2O_3 nanorods, and (c) the γ-Fe_2O_3 nanorods.

Thermal calcination of the as-prepared β-FeOOH at 500 °C in air yielded α-Fe_2O_3 nanorods. As shown in Figure 1b, the diffraction lines of β-FeOOH vanished completely while the reflections representing α-Fe_2O_3 (ICSD 64599) appeared, implying that the oxyhydroxide has been dehydrated to ferric oxide. It is noteworthy that the intensities of the (104) to (110) lines were much lower than those in the standard card, indicative of the anisotropic size effect.[22] In the FTIR spectrum (Figure 2b), α-Fe_2O_3 exhibited two strong absorption bands centered at 470 and 538cm^{-1}, being the framework vibrations of Fe-O-Fe.[23] As shown in Figure 4, the obtained α-Fe_2O_3 had the rod-like shape with the diameter of 30-40 nm and the length of 400-500 nm. Differing from the β-FeOOH precursor, the α-Fe_2O_3 nanorods had coarser surfaces and mesopores with an average size of 20 nm, perhaps because of the fast dehydration rate.[24] The interplanar spacing of 0.251 and 0.145 nm on the HRTEM image corresponded to the *d*-values of the $(\bar{2},10)$ and (030) planes, respectively, with a dihedral angle of 30°. Taking the rectangular tip into account, the α-Fe_2O_3 nanorod was determined to have two $\{\bar{2},10\}$ and two {001} side-planes and two {010} top planes. Alpha-Fe_2O_3 has a corundum-type structure (space group $R\bar{3}ch(167)$) with lattice parameters of 0.50352 and 1.37508 nm,[25] in which the Fe^{3+} ions occupy two-thirds of the octahedral sites that are confined by the nearly ideal hexagonal close-packed O lattice along the [001] direction.[1, 26] On this basis, the exposed $\{\bar{2},10\}$ and {001} side planes the α-Fe_2O_3 nanorods are Fe-terminated surfaces without O anions; only the minor top {010} planes are composed of Fe cations and O anions.

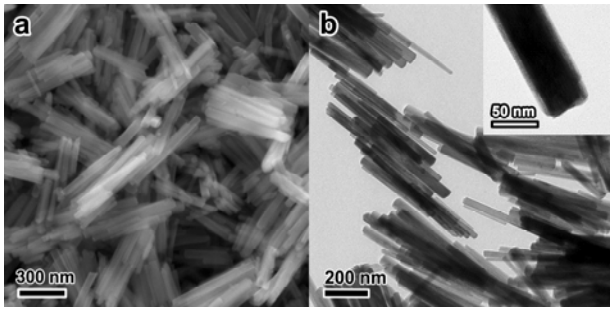

Figure 3. SEM/TEM images of the β-FeOOH precursor.

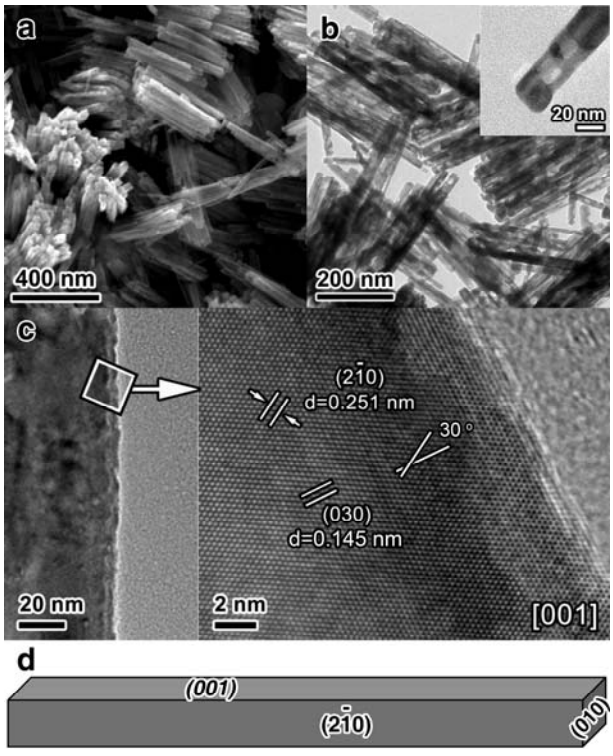

Figure 4. SEM/TEM images of the α-Fe_2O_3 nanorods.

When the β-FeOOH precursor was refluxed in PEG at 200 °C, interestingly, γ-Fe_2O_3 nanorods were formed. The XRD pattern (Figure 1c) exhibited diffraction lines of γ-Fe_2O_3 (ICSD 172905).

Compared with the intensities of the standard XRD pattern of γ-Fe_2O_3, the intensities of the (400) and (440) lines enhanced significantly but those of the (422) and (511) lines weakened largely, suggesting the preferential exposure of the {110} and {100} planes. To further discriminate γ-Fe_2O_3 and Fe_3O_4, the $Fe^{2+}/(Fe^{2+}+Fe^{3+})$ ratio was estimated to be 0.044 by a redox titration process,[27] reaffirming that the β-FeOOH precursor was exclusively converted to γ-Fe_2O_3, instead of Fe_3O_4. In addition, the bands at 561 and 632 cm^{-1} in the FTIR spectrum (Figure 2c) also evidenced the formation of γ-Fe_2O_3 because Fe_3O_4 has absorption bands at 390 and 570cm^{-1}.[28] SEM and TEM observations (Figure 5) verified the rod-like morphology with an average diameter of 40 nm and a mean length of 400 nm. The nanorod had a regular rectangle cross-section with the length of 50 nm and the width of 40 nm. The γ-Fe_2O_3 nanorods also had mesopores of about 22 nm in diameter but the pores were more uniform and well arranged when compared to those on the α-Fe_2O_3 nanorods. The mesopores that were generated during the dehydration process had an open structure and were isolated from each other. HRTEM observation further identified the crystallographic property of the γ-Fe_2O_3 nanorods. When viewed along the [1¯,25] direction (Figure 5c), three lattice fringes of 0.373, 0.341 and 0.253 nm were clearly observed, which corresponded to the (210), (1¯,21) and (311)/(131) planes, respectively. The lattice fringes of 0.297 and 0.417 in Figure 5d represented the (220) and (002) planes with a dihedral angle of 90°, indicating that the nanocrystal grew along the [110] direction. Apparently, the γ-Fe_2O_3 nanorod had {1¯,10} and {001} side planes and {220} top plane (Figure 5d). Gamma-Fe_2O_3 possesses a cubic structure with a lattice constant of 0.83474 nm (space group, Fd3m),[1, 29] in which the oxygen anions have a cubic close-packed array and the Fe^{3+} ions distribute over the tetrahedral sites and the octahedral sites. Based on this atomic configuration, both the iron cations and the oxygen anions existed simultaneously on the exposed {1¯,10} and {001} planes of the γ-Fe_2O_3 nanorods.

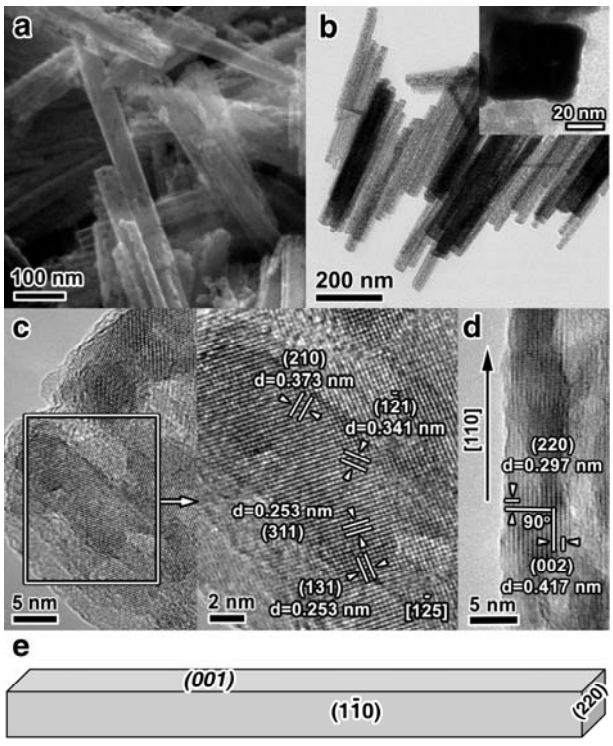

Figure 5. SEM/TEM images of the γ-Fe_2O_3 nanorods.

Phase transformation

β-FeOOH has a tetragonal structure (body-centered cubic packed array, bcp) consisting of double chains of edge-shared octahedra that are parallel to the c axis with Fe^{3+} ions in octahedral sites.[30] The neighboring double chains are corner-shared to form a three-dimensional tunnel structure. Therefore, the transition of β-FeOOH to Fe_2O_3 involves a complete structural destruction of the less tense packed anions at first and then a re-construction of the anion arrays, being strongly dependent on the crystallinity of β-FeOOH. Here, α- and γ-Fe_2O_3 nanorods were obtained from the oxyhydroxide precursor by thermal heating and refluxing in PEG, respectively. The square-like tips of the β-FeOOH nanorods, differing from the traditional round tips,[30] indicated the well crystallinity nature that may induce unique dehydration pattern. Generally, the dehydration process is related to the content of water in the surrounding atmosphere and higher water content often requires a higher transformation temperature. [31] When the β-FeOOH precursor was heated in air, α-Fe_2O_3 was produced by the fast dehydration process as expected.[32] However, refluxing in PEG together with the continuous flow of nitrogen resulted in the formation of γ-Fe_2O_3 probably because of the very low water content and the slightly reducing environment.

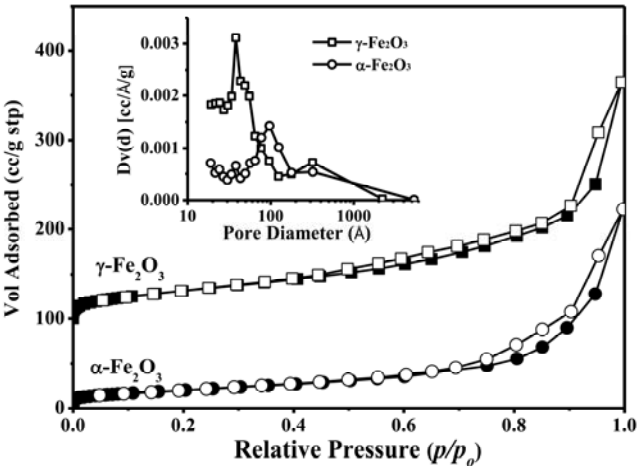

Figure 6. N_2 adsorption/desorption isotherms and pore size distributions of the α- and γ-Fe_2O_3 nanorods.

Figure 6 compares the nitrogen adsorption/desorption isotherms of the Fe_2O_3 nanorods. The isotherms were Type IV adsorptions with H3 hysteresis loops, indicating the presence of mesopores constructed by the aggregation of Fe_2O_3 nanoparticles.[24] The specific surface areas of the α- and γ-Fe_2O_3 nanorods were 79 and 120 m^2/g, respectively. The pore size distribution of the α-Fe_2O_3 nanorods showed two peaks centered at 10 and 30 nm, while a strong peak at 3 nm and a weak peak at 30 nm were observed over the γ-Fe_2O_3 nanorods. This result confirms that the pore size distribution was more uniform on the γ-Fe_2O_3 nanorods than that over the α-Fe_2O_3 nanorods, as observed from their TEM images. As mentioned above, β-FeOOH possesses a tunnel-like structure that is filled with water. Upon calcination, water was rapidly removed from the tunnels and the subsequent solid-state-transformation resulted in the formation of larger mesopores on the α-Fe_2O_3 nanorods. In contrast, the dehydration process in PEG solution proceeded very slowly and mildly at the lower temperature, generating uniform mesopores on the γ-Fe_2O_3 nanorods.

Figure 7 compares the H_2-TPR profiles of the α-Fe_2O_3 and γ-Fe_2O_3 nanorods. Both samples showed very similar reduction behavior consisting of two distinctive steps. The first reduction

peak below 400 °C was due to the reduction of Fe_2O_3 to Fe_3O_4 while the broad peak at above 400 °C represented the further reduction of Fe_3O_4 to metallic iron, perhaps through FeO.[33] The total amounts of hydrogen consumed were 19.76 mmol H_2/g for the α-Fe_2O_3 nanorods and 18.24 mol H_2/g for the γ-Fe_2O_3 nanorods, being approximately equal to the stoichiometric amount required for Fe_2O_3 reduction to Fe (18.75 mol H_2/g). In particular, the hydrogen amounts consumed by the low-temperature reduction peak took about 15% of the total amount in both cases. They were slightly greater than that of bulk ferric oxide (11.1%) because of nanosized effect.[34] Notably, the temperature for the occurrence of the initial reduction shifted from 300 °C on the γ-Fe_2O_3 nanorods to 360 °C on the α-Fe_2O_3 nanorods, suggesting the facile reduction of the γ-Fe_2O_3 nanorods. This easier reduction of the gamma crystal phase is of utmost importance in chemical reactions involving a redox cycle.[35]

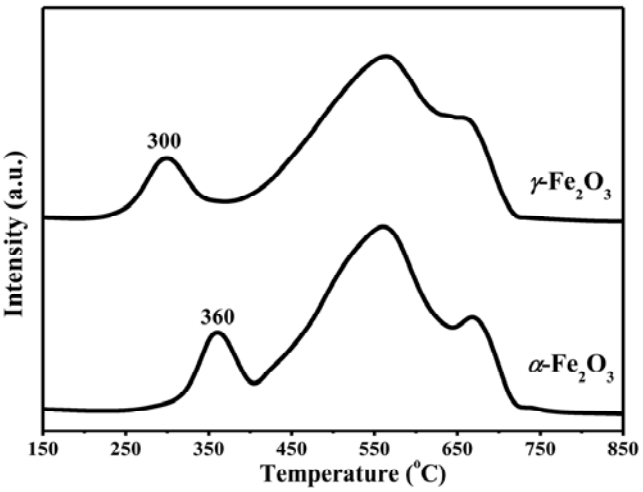

Figure 7. H_2-TPR profiles of the α- and γ-Fe_2O_3 nanorods.

NO reduction by CO

Reduction of NO by CO is one of the key reactions in the three-way catalytic converter for abating the exhaust from gasoline-fuelled engines, where noble metals such as Pd, Pt, and Rh, are currently used as the major catalytic components.[36] To explore less expensive and more efficient catalytic materials, metal oxides as the potential catalysts have been extensively investigated for this environmentally important reaction.[37] Figure 8a illustrates the catalytic performance of the Fe_2O_3 nanorods for NO reduction by CO. The reaction readily started at 175 °C on the γ-Fe_2O_3 nanorods but it occurred at 325 °C over the α-Fe_2O_3 nanorods. At 500 °C, the conversion of NO approached 95% on the γ-Fe_2O_3 nanorods, being much higher than that on the α-Fe_2O_3 nanorods (40%). These results clearly demonstrated the outstanding performance of the γ-Fe_2O_3 nanorods. More importantly, the selectivity of N_2 was as high as 100% on both samples without the formation of N_2O that is frequently formed on noble metals.[38] Long-term stability tests were then conducted at 400 °C (Figure 8b). On the γ-Fe_2O_3 nanorods, the conversion of NO maintained at about 80% during the whole operation. However, the conversion of NO was only increasing from 20% at the initial stage to 40% at the end of 100 h on-stream over the α-Fe_2O_3 nanorods.

To elucidate the catalytic properties of the Fe_2O_3 nanorods, NO-TPD tests were performed (Figure 9). On the α-Fe_2O_3 nanorods, two NO desorptions appeared at 63 and 113 °C, being simply ascribed to the physically adsorbed NO molecules. On the γ-Fe_2O_3 nanorods, in addition to the low-temperature NO desorptions, two additional NO desorptions occurred at 169 and 220 °C, indicating the presence of strongly and/or chemically adsorbed NO molecules. This is related with the surface properties of the γ-Fe_2O_3 nanorods where the neighboring oxygen ions facilitated NO adsorption and activation on the ferric site.[39] This kind of strong adsorption hardly occurred on the surface of the α-Fe_2O_3 nanorods that were terminated by ferric ions alone. NO reduction by CO on Fe_2O_3 follows a typical redox process;[40] CO is to reduce Fe_2O_3 for maintaining a sufficient concentration of surface oxygen vacancies for the occurrence of NO reduction. The exposing facets of the α- and γ-Fe_2O_3 nanorods have different distributions of surface ferric and oxygen ions. The ferric ions on the α-Fe_2O_3 nanorods provided adsorption sites for NO molecule only, while the co-existence of ferric and oxygen ions on the surface of the γ-Fe_2O_3 nanorods not only enhanced the adsorption and activation of NO molecules but facilitated of NO reduction by CO through a redox cycle. As a result, the γ-Fe_2O_3 nanorods are characterized by the remarkably improved reaction activity. We have recently also demonstrated that this γ-phase structure is very active and stable in selective catalytic reduction of NO by NH_3.[41]

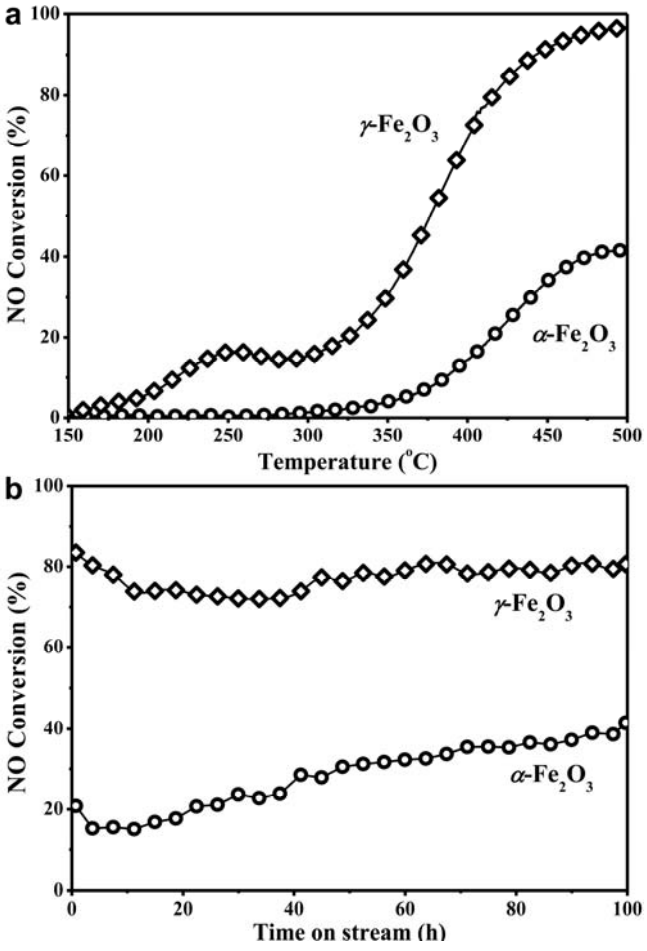

Figure 8. NO conversions as a function of temperature (a) and time on-stream (b) on the α- and γ-Fe_2O_3 nanorods.

Conclusions

Porous α- and γ-Fe_2O_3 nanorods having similar morphology but different crystal phases have been prepared by proper dehydration of a rod-shaped β-FeOOH precursor that was obtained by a

controlled precipitation process in aqueous phase. Calcination of the β-FeOOH nanorods in air produced α-Fe_2O_3 nanorods but refluxing in PEG solution yielded γ-Fe_2O_3 nanorods. Because of the different crystalline structures, the α-Fe_2O_3 nanorods mainly exposed the $\{2^{-},10\}$ and {001} facets that were terminated by ferric ions only while the γ-Fe_2O_3 nanorods preferentially exposed the {110} and {001} facets which were co-terminated by iron and oxygen ions. The γ-Fe_2O_3 nanorods were much more active for NO reduction by CO than the α-Fe_2O_3 nanorods because the exposed facets effectively adsorbed and activated NO and CO molecules.

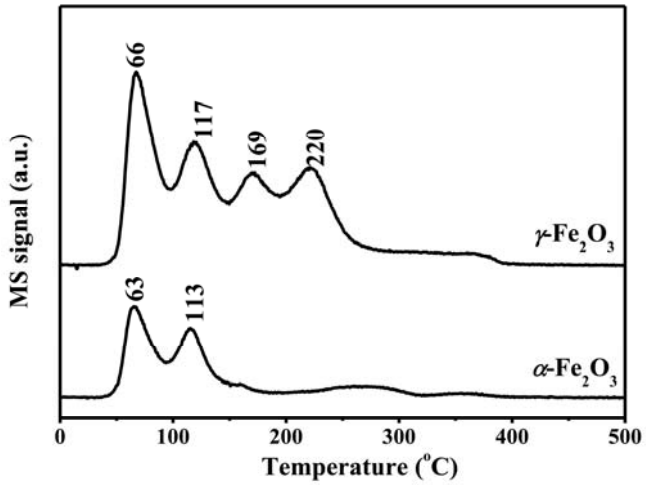

Figure 9. NO-TPD profiles of the α- and γ-Fe_2O_3 nanorods.

Experimental Section

Materials preparation: All reagents were commercially available in analytical purity and used without further purification. A solution containing 0.02 mol $FeCl_3 \cdot 6H_2O$, 0.2 mol NaCl, 10 mL polyethylene glycol (PEG, molecule weight = 400) and 190 mL H_2O was gradually heated to 120 °C under mechanical stirring and maintained at that temperature for 1 h. Then 200 mL of 0.2 M Na_2CO_3 aqueous solution was pumped continuously at a rate of 5.6 mL/min into the mixed solution at 120 °C. The precipitate was aged in the mother liquid for another 1 h. After filtration and being washed with deionized water and ethanol, the obtained solid was dried at 50 °C for 6 h under vacuum. α-Fe_2O_3 was obtained by calcining the β-FeOOH nanorods at 500 °C in air for 5 h. γ-Fe_2O_3 was prepared by refluxing the β-FeOOH nanorods in PEG solution. 5.0 g of the as-prepared β-FeOOH was dispersed into 500 mL PEG and the mixture was gradually heated to 200 °C with mechanical stirring under N_2 flow. After refluxing for 24 h, the precipitate was filtrated and washed thoroughly with water and ethanol, followed by drying in vacuum at 50 °C for 6 h.

Structural analyses: X-ray powder diffraction (XRD) patterns were recorded on a D/Max-2500/PC powder diffractometer (Rigaku, Japan) operated at 40 kV and 300 mA, using a nickel-filtered Cu K_α (0.15418 nm) radiation source. N_2-adsorption-desorption isotherms were recorded at 77 K on a Micromeritics ASAP 2010 instrument. Before the measurement, the sample was degassed at 300 °C for 6 h. The BET surface area was calculated from a multipoint BET analysis of the nitrogen adsorption isotherm, and the size distribution was estimated by the BJH method. Transmission electron microscopy (TEM) images were taken on a Philips FEI Tecnai G^2 microscopy operating at an accelerating voltage of 120 kV, and high resolution TEM (HRTEM) images were obtained on a FEI Tecnai G2 F30S-Twin microscope operated at an accelerating voltage of 300 kV. The specimen was prepared by ultrasonically dispersing the sample into ethanol, and droplets of the suspensions were deposited on a carbon-enhanced copper grid and then dried in air. Field emission scanning electron microscopy (FESEM) images were taken using a Philips FEI Quanta 200F instrument operated at 20-30 kV. The samples were placed on a conductive carbon tape adhered to an aluminum sample holder. Temperature-programmed desorption of NO (NO-TPD) was carried out with a microreactor equipped with an on-line mass spectrometer (Omini-star, QMG 220, Balzers). 100 mg of iron oxide sample was pre-treated with a He flow (30 mL/min) at 400 °C for 0.5 h to remove the surface impurities. After being cooled to room temperature under He flow, the sample was exposed to a mixture of 1000 ppm NO/He (mL/min) for 1 h. Subsequently, the sample was flushed with He (30 mL/min) for another 1 h and heated to 500 °C at a rate of 5 °C/min. The effluent was monitored by mass spectrometer at m/e of 28(N_2), 30(NO), 44(N_2O) and 46(NO_2).

NO reduction by CO: NO reduction by CO was conducted in a fixed-bed quartz tubular reactor under atmospheric pressure. 100 mg samples (40–60 mesh) were placed between two plugs of quartz wool and then pre-treated with pure He (30 mL/min) at 400 °C for 0.5 h. After cooling to room temperature, a 0.5% NO/0.5% CO/He mixture (30 mL/min) was introduced through a mass flow controller. The reactor was then heated from room temperature to 500 °C with a ramp rate of 1 °C/min. The effluent from the reactor was analyzed by on-line gas chromatographs equipped with thermal conductivity detector using Molecular Sieve 5A and Porapak Q columns. A $NO/NO_2/NO_x$ analyzer (Model 42i, Thermo Environmental Instruments Inc.) was also employed to monitor the concentrations of NO and NO_2. NO conversion was calculated according to the following equation:

$$\text{NO Conversion\%} = ([NO]_{in} - [NO]_{out}) \times 100/[NO]_{in}$$

Acknowledgments

We acknowledge the financial support for this research work from the National Nature Science Foundation of China (20923001 and 21025312).

[1] L. Machala, J. Tuček, R. Zbořil, *Chem. Mater.* **2011**, *23*, 3255-3272.

[2] A. Navrotsky, L. Mazeina, J. Majzlan, *Science* **2008**, *319*, 1635-1638.

[3] H. G. Cha, S. J. Kim, K. J. Lee, M. H. Jung, Y. S. Kang, *J. Phys. Chem. C* **2011**, *115,* 19129-19135.

[4] H. Sharghi, M. Jokar, M. M. Doroodmand, R. Khalifeh, *Adv. Synth. Catal.* **2010**, *352*, 3031-3044.

[5] K. Sivula, F. Le Formal, M. Grätzel, *ChemSusChem* **2011**, *4*, 432-449.

[6] a) M. I. Shukoor, F. Natalio, N. Metz, N. Glube, M. N. Tahir, H. A. Therese, V. Ksenofontov, P. Theato, P. Langguth, J. P. Boissel, H. C. Schroder, W. E. G. Muller, W. Tremel, *Angew. Chem. Int. Edit.* **2008**, *47*, 4748-4752; b) M. I. Shukoor, F. Natalio, H. A. Therese, M. N. Tahir, V. Ksenofontov, M. Panthofer, M. Eberhardt, P. Theato, H. C. Schroder, W. E. G. Muller, W. Tremel, *Chem. Mater.* **2008**, *20*, 3567-3573.

[7] M. Tadić, D. Marković, V. Spasojević, V. Kusigerski, M. Remškar, J. Pirnat and Z. Jagličić, *J. Alloy. Compd.* **2007**, *441*, 291-296.

[8] S. Wang, Y. Min, S. Yu, *J. Phys. Chem. C* **2007**, *111*, 3551-3554.

[9] a) A. B. Bourlinos, A. Simopoulos, D. Petridis, *Chem. Mater.* **2002**, *14*, 899-903; b) G. Gnanaprakash, S. Ayyappan, T. Jayakumar, J. Philip, B. Raj, *Nanotechnology* **2006**, *17*, 5851-5857; c) D. Li, W. Y. Teoh, C. Selomulya, R. C. Woodward, R. Amal, B. Rosche, *Chem. Mater.* **2006**, *18*, 6403-6413.

[10] a) K. Woo, H. J. Lee, J. P. Ahn, Y. S. Park, *Adv. Mater.* **2003**, *15*, 1761-1764; b) Z. Zhong, J. Ho, J. Teo, S. Shen, A. Gedanken, *Chem. Mater.* **2007**, *19*, 4776-4782; c) T. P. Almeida, M. Fay, Y. Zhu, P. D. Brown, *J. Phys. Chem. C* **2009**, *113*, 18689-18698.

[11] a) L. Vayssieres, C. Sathe, S. M. Butorin, D. K. Shuh, J. Nordgren, J. Guo, *Adv. Mater.* **2005**, *17*, 2320-2323; b) J. S. Jang, K. Y. Yoon, X. Xiao, F. R. F. Fan, A. J. Bard, *Chem. Mater.* **2009**, *21*, 4803-4810.

[12] a) C. J. Jia, L. D. Sun, Z. G. Yan, L. P. You, F. Luo, X. D. Han, Y. C. Pang, Z. Zhang, C. H. Yan, *Angew. Chem. Int. Edit.* **2005**, *44*, 4328-4333; b) S. K. Mohapatra, S. E. John, S. Banerjee, M. Misra, *Chem. Mater.* **2009**, *21*, 3048-3055.

[13] U. Cvelbar, Z. Q. Chen, M. K. Sunkara, M. Mozetic, *Small* **2008**, *4*, 1610-1614.

[14] Y. M. Zhao, Y. H. Li, R. Z. Ma, M. J. Roe, D. G. McCartney, Y. Q. Zhu, *Small* **2006**, *2*, 422-427.

[15] C. Wu, P. Yin, X. Zhu, C. OuYang, Y. Xie, *J. Phys. Chem. B* **2006**, *110*, 17806-17812.

[16] P. C. Wu, W. S. Wang, Y. T. Huang, H. S. Sheu, Y. W. Lo, T. L. Tsai, D. B. Shieh, C. S. Yeh, *Chem. Eur. J.* **2007**, *13*, 3878-3885.

[17] Q. Han, Z. H. Liu, Y. Y. Xu, Z. Y. Chen, T. M. Wang, H. Zhang, *J. Phys. Chem. C.* **2007**, *111*, 5034-5038.

[18] J. Wang, Y. Ma, K. Watanabe, *Chem. Mater.* **2008**, *20*, 20-22.

[19] J. Cheon, N. J. Kang, S. M. Lee, J. H. Lee, J. H. Yoon, S. J. Oh, *J. Am. Chem. Soc.* **2004**, *126*, 1950-1951.

[20] E. A. Deliyanni, D. N. Bakoyannakis, A. I. Zouboulis, K. A. Matis, L. Nalbandian, *Microporous Mesoporous Mat.* **2001**, *42*, 49-57.

[21] H. Yu, X. Song, Z. Yin, W. Fan, X. Tan, C. Fan, S. Sun, *J. Nanopart. Res.* **2007**, *9*, 301-308.

[22] N. Pailhe, J. Majimel, S. Pechev, P. Gravereau, M. Gaudon, A. Demourgues, *J. Phys. Chem. C* **2008**, *112*, 19217-19223.

[23] I. V. Chernyshova, M. F. Hochella Jr, A. S. Madden, *Phys. Chem. Chem. Phys.* **2007**, *9*, 1736.

[24] M. Chen, J. Jiang, X. Zhou, G. Diao, *J. Nanosci. Nanotechnol.* **2008**, *8*, 3942-3948.

[25] C. J. Jia, L. D. Sun, F. Luo, X. D. Han, L. J. Heyderman, Z. G. Yan, C. H. Yan, K. Zheng, Z. Zhang, M. Takano, N. et al., *J. Am. Chem. Soc.* **2008**, *130*, 16968-16977.

[26] X. L. Hu, J. C. Yu, *Adv. Funct. Mater.* **2008**, *18*, 880-887.

[27] M. Ai, E. Muneyama, A. Kunishige, K. Ohdan, *Appl. Catal. A-Gen.* **1994**, *109*, 135-146.

[28] A. A. Khaleel, *Chem. Eur. J.* **2004**, *10*, 925-932.

[29] J.-E. Jørgensen, L. Mosegaard, L. E. Thomsen, T. R. Jensen, J. C. Hanson, *J. Solid State Chem.* **2007**, *180*, 180-185.

[30] R. M. Cornell, U. Schwertmann, *The iron oxides: structure, properties, reactions, occurrence and uses*, (2nd edition), *Chapt. 14*, Wiley-VCH, Weinheim, **2003**, pp. 365-405.

[31] L. Mazeina, S. Deore, A. Navrotsky, *Chem. Mater.* **2006**, *18*, 1830-1838.

[32] a) Music, S., *Mater. Lett.* **2004**, *58*, 444-448; b) N. K. Chaudhari, J. S. Yu, *J. Phys. Chem. C* **2008**, *112*, 19957-19962.

[33] a) S. J. Hug, *J. Colloid Interface Sci.* **1997**, *188*, 415-422; b) J. Zieliński, I. Zglinicka, L. Znak, Z. Kaszkur, *Appl. Catal. A-Gen.* **2010**, *381*, 191-196.

[34] W. K. Jozwiak, E. Kaczmarek, T. P. Maniecki, W. Ignaczak, W. Maniukiewicz, *Appl. Catal. A-Gen.* **2007**, *326*, 17-27.

[35] H. Randall, R. Doepper, *A. Renken, Ind. Eng. Chem. Res.* **1997**, *36*, 2996-3001.

[36] a) V. I. Parvulescu, P. Grange, B. Delmon, *Catal.Today* **1998**, *46*, 233-316; b) Chafik, T., *J. Catal.* **2000**, *190*, 446-459; c) M. Crocoll, S. Kureti, W. Weisweiler, *J. Catal.* **2005**, *229*, 480-489; d) P. Schmitz, R. Kudla, A. Drews, A. Chen, C. Lowema, R. McCabe, W. Schneider, C. Goralskijr, *Appl. Catal. B-Environ.* **2006**, *67*, 246-256.

[37] a) Y. Okamoto, T. Kubota, Y. Ohto, S. Nasu, *J. Catal.* **2000**, *192*, 412-422; b) T. Rühle, O. Timpe, N. Pfänder, R. Schlögl, *Angew. Chem. Int. Edit.* **2000**, *39*, 4379-4382; cM. Natile, *J. Mol. Catal. A-Chem.* **2004**, *217*, 175-184; d) Y. Hu, L. Dong, M. Shen, D. Liu, J. Wang, W. Ding, Y. Chen, *Appl. Catal. B-Environ.* **2001**, *31*, 61-69.

[38] J. A. Wang, A. Cuan, J. Salmones, N. Nava, S. Castillo, M. Morán-Pineda, F. Rojas, *Appl. Surf. Sci.* **2004**, *230*, 94-105.

[39] G. V. Glazneva, I. S. Sazonova, Y. M. Shchekochikhin, A. A. Davydov, N. P. Keier, *React. Kinet. Catal. Lett.* **1978**, *9*, 131-136.

[40] H. Randall, R. Doepper, A. Renken, *Appl. Catal. B-Environ.* **1998**, *17*, 357-369.

[41] X. Mou, B. Zhang, Y. Li, L. Yao, X. Wei, D. S. Su, W. Shen, *Angew. Chem. Int. Edit.*, submitted.

Received: ((will be filled in by the editorial staff))
Published online: ((will be filled in by the editorial staff))

Entry for the Table of Contents

((Key Topic))

Alpha- and gamma-Fe_2O_3 nanorods were obtained by proper dehydration of a rod-shaped *β*-FeOOH precursor, and the Fe_2O_3 nanorods showed distinct crystal phase effect in NO+CO reaction based on their exposed surface facets.

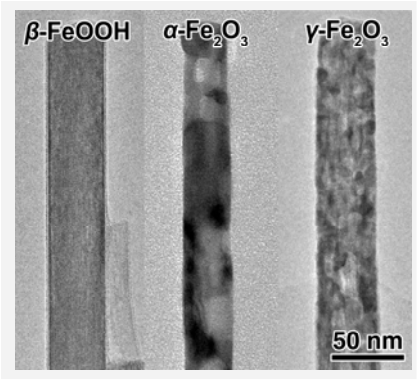

Xiaoling Mou, [a] Yong Li, [a] Bingsen Zhang, [b] Lide Yao, [b] Xuejiao Wei, [a], Dang Sheng Su* [b,c] and Wenjie Shen* [a]…….. Page No. – Page No.

Crystal phase and morphology controlled synthesis of Fe_2O_3 nanomaterials

Keywords: Crystal Phase / Fe_2O_3 / Morphology / Nanorods / NO+CO